Proceedings of the 17th IEEE International
Conference on Nano/Micro Engineered and Molecular Systems
April 14-17, 2022

2022 IEEE 17th International Conference on Nano/Micro Engineered and Molecular Systems (NEMS) | 978-1-6654-8301-8/22/$31.00 ©2022 IEEE | DOI: 10.1109/NEMS54180.2022.9791201

Fabrication of Solid Microneedle using Multi-slit Diffraction UV Lithography

Jun Ying Tan, Yuankai Li, Punit Prakash, Bala Natarajan, and Jungkwun 'JK' Kim
Department of Electrical and Computer Engineering, Kansas State University, Manhattan K.S. 66506 USA.
justintan@ksu.edu, yuankai@ksu.edu, prakashp@ksu.edu, bala@ksu.edu, and jkkim1324@ksu.edu

***Abstract*— This paper presents multi-slit diffraction lithography for fabricating legs-supported microneedles. Various micropatterns as multiple slits enable the combination of multiple distinct UV light rays to generate the leg-supported microneedle in a liquid state photosensitive resin. This paper investigates the impact of the number of slits including double, triple and quadruple patterns on the shape of the microneedle. Additionally, the effect of the microslits distance on the microneedle shape is also quantified. The investigation result leads to overall cleaner leg separations and shorter microneedle height with increasing slit distances. Mechanical testing of the fabricated microneedles revealed a tip strength of 0.5 N, confirming their functionality as a microneedle. Featuring the physical separation of the microneedle legs, a resistive heating microneedle device was fabricated and characterized. Temperatures of up to 95 °C were detected without causing substantial damage to the tip, indicating a major potential for targeted heat treatment in tissue engineering.**

Keywords—microneedles, diffraction UV lithography, multi-slit, micro-heaters, photosensitive resin

I. Introduction

Microneedles have gained growing popularity as a transdermal drug delivery method due to their minimally invasive nature [1]. Moreover, microneedles have been investigated as an advanced multimodal sensing platform for glucose [2], oxygen [3], interstitial fluid [4], and therapeutic drugs [5]. To achieve the multi-functionality of the microneedle, not only high precision fabrication is necessary, the process should also be compatible with other conventional procedures such as micropatterning or metallization. However, typical microneedle production techniques such as micromolding or etching have not been widely used for the advanced microneedle functional platform due to the limited adaptability provided by the need for master mold or the high cost associated with the dry or laser etching processes. To overcome the challenges, high precision fabrication methods for microneedles that supports micropatterning and metallization have been reported recently including drawing lithography [6], three-dimensional (3D) printing [7] and two-photon polymerization [8]. Drawing lithography has demonstrated a great batch fabrication process and feasibility for realizing microneedles with multi-functionality [6], [9]. However, the precise control of the microneedle shape was challenging due to the nature of the material pulling fabrication process, which is solely practical to fabricate specific microneedle shapes that hinder the functional availability of the microneedle. Alternatively, 3D printing has been widely known to have vast customizability for fabricating complex 3D structures within hours. Wide varieties of biocompatible 3D printable materials also expand the practicality of 3D printing in developing microneedle-based sensing devices [10]. However, the major challenge when adopting 3D printing for microneedle fabrication boils down to its inevitable step effect on the needle body and relatively low tip sharpness (<20 µm). These deficiencies prohibited 3D printing from being applicable for fabricating multi-functional microneedles. On the other hand, an advanced 3D printing technique known as the two-photon polymerization has demonstrated promising results in fabricating microneedles with relatively smooth surface profile and sharp needle tip with moderate aspect ratio, which are crucial characteristics for realizing multi-functional microneedles. However, the need for high-cost equipment and relatively slow printing speed due to laser-based additive manufacturing techniques, hampers the popularization of multi-functional microneedles.

Ultraviolet (UV) lithography as a fundamental nano/micropatterning technique has been widely employed in industry and research for decades. While conventional UV lithography has been primarily used for two-dimensional (2D) micropatterning, advancements of UV lithography have demonstrated potential results in fabricating even millimeter tall 3D microstructures [11]–[13]. Recently, we found that the unique cone was formed when the collimated UV light directly exposed to the liquid state photosensitive resin through a small slit, e.g., photomask pattern [14]. More recently, we have claimed this unique cone forming principle as a diffraction lithography for microneedle fabrications [15]–[17]. The microneedle shape is formed through the diffracted light distribution in the photosensitive liquid state resin. This diffraction lithography technology demonstrated different types of microneedles including various height solid microneedles, a hollowed microneedles, and inclined microneedles proving the feasibility of producing a simple and accurate microneedle. Leveraging our earlier works, this paper introduces a novel multi-slit diffraction lithography approach for fabricating

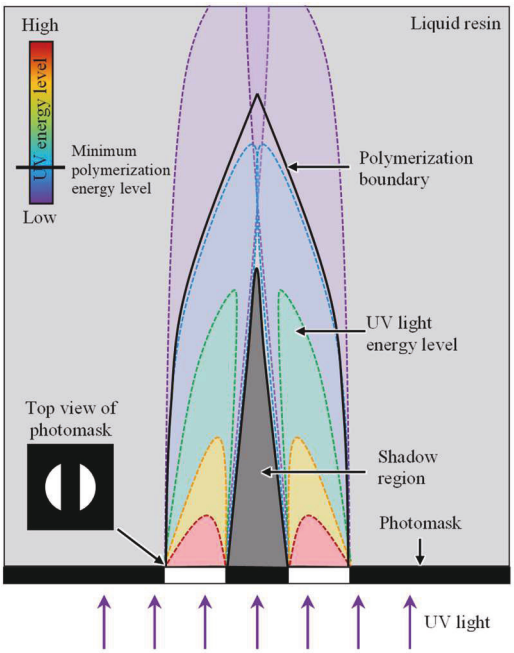

Fig. 1. Conceptual drawing of the UV light propagation through double-slit micro-patterns and its polymerization boundary to form the microneedle.

Research was supported by National Science Foundation CNS 2039014, ECCS, 2054567, and ECCS, 2029086.

unique, multi-leg supported, high aspect ratio microneedles. While earlier works have mainly explored the single micropattern-based diffraction phenomena, this paper has introduced the diffraction from the multi-slits, e.g., multiple micropatterns on the photomask, that generated a unique merging light propagation as described in Fig.1. The light propagation inside the photosensitive resin was demonstrated to show the legs-supported microneedle. Various microneedle shapes based on the distance among the micropatterns and the number of patterns were experimentally verified. The force-displacement test also proved that the fabricated microneedles could be used for skin insertions. The introduced multi-slits diffraction lithography has successfully fabricated unique legs-supported microneedles and tested as a heat stimulation microneedle device.

II. Fabrication Process

The fabrication process of the multi-leg microneedle that is also associated with the multi-slit diffraction lithography is depicted in Fig 2. The photomask patterning including double, triple, and quadruple micropatterns was prepared using a mask writer (SF-100 XPRESS, Scotech Co., Ltd.) on a chromium coated glass (soda-lime glass, Telic company) as shown in Fig. 2(a). The photomask was placed on a resin tank filled with liquid photosensitive resin (Surgical Guide Resin, Formlabs Inc.) as shown in Fig. 2(b). The collimated UV light was applied to the photomask side as described in Fig. 2(c). The UV light through the photomask was diffracted inside the liquid resin and crosslinked the UV exposed region of the liquid resin. No mask alignment procedure was needed for the UV exposure process since the photomask was used as the substrate to prevent complications. Once the UV exposure process is complete, the microneedles should be facing downwards while remaining intact with the photomask as shown in Fig. 2(d). The sample was removed carefully from the resin tank and cleaned with isopropanol to remove excess liquid resin as shown in Fig. 2(e). The cleaned sample was dried with compressed air, and the multi-leg microneedle is complete as shown in Fig. 2(f).

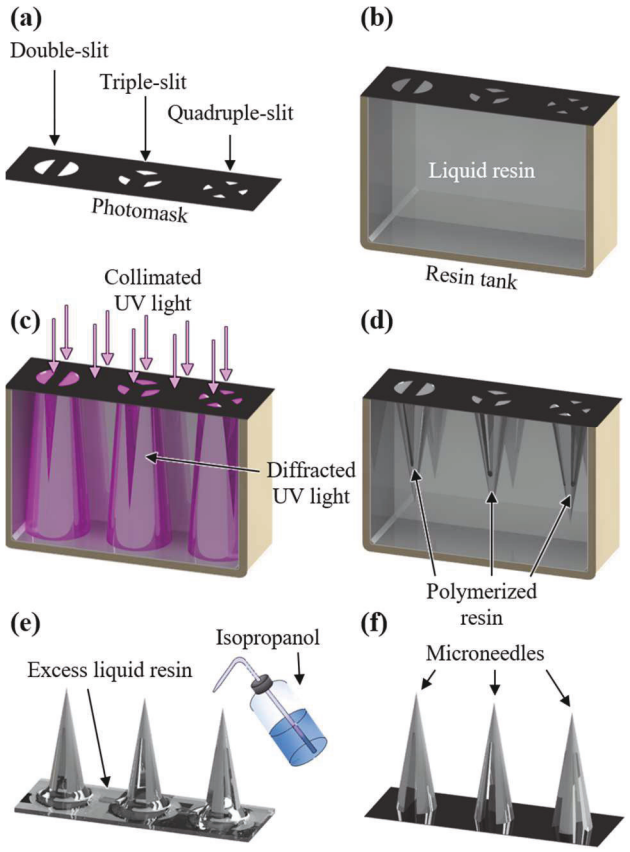

Fig. 2. Fabrication process of the multi-leg microneedle. (a) Photomask design. (b) Placing photomask on the resin tank. (c) UV exposure. (d) Selective polymerization after UV exposure. (e) Clean sample with isopropanol. (f) Multi-leg microneedle complete.

III. Results

UV light propagation via double-slit micro-patterns inside the liquid photosensitive resin was experimentally visualized as shown in Fig. 3. The progress of the polymerization of the photosensitive resin was photographed via UV exposure time. Fig. 3(a) shows the 45° angled front view of two semi-circle micro-patterns (double-slit) with a diameter of 500 µm and a gap of 170 µm. UV light was introduced through the micro-patterns prior to resin coating as an initial condition. The UV light propagation on the micro-patterns during the polymerization process over time is presented in Fig. 3(b) to (d). The initial light propagation in Fig. 3(b) shows the individual diffraction from each micro-pattern. The height of the diffracted light was about 1.2 mm. When the polymerization started, the UV light was clearly guided inwards and combined into a single light beam in Fig. 3(c), which indicates two supporting legs of the microneedle has been completed. The height of the diffracted light at this point was measured to be 1.4 mm in Fig. 3(c), which was later confirmed by measuring the height of the microneedle legs as shown in Fig 3(e). Fig. 3(d) shows the UV light propagation after merging to form the tip with a final height of 1.8 mm, which also agrees with the measured height of the microneedle as shown in Fig. 3(e). Fig. 3(e) shows the fabrication result obtained by pausing the exposure for 120 seconds. The result of the experiment validates that the shape of the microneedles strongly correlates with UV light propagation.

The effect of the slit distance and the number of slits to the shape of the multi-leg microneedle was investigated. Double-,

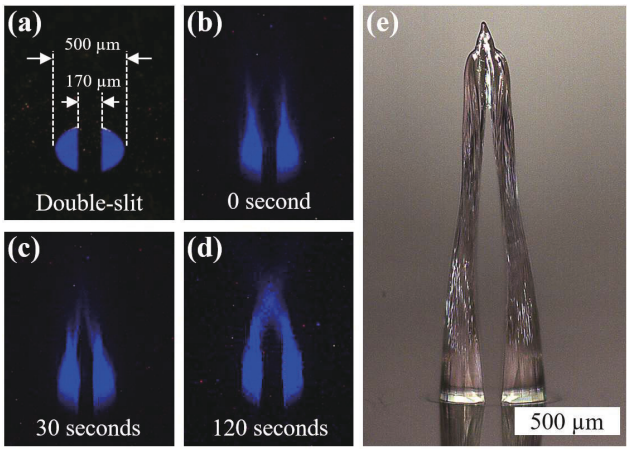

Fig. 3. UV light propagation through a double-slit micro-pattern before and after resin coating and fabrication result. (a) Micro-pattern before resin coating. UV light propagation at (b) 0 s (right after resin coating), (c) 30 s, (d) 120 s. (e) Double-leg microneedle with 120 s UV exposure after wash.

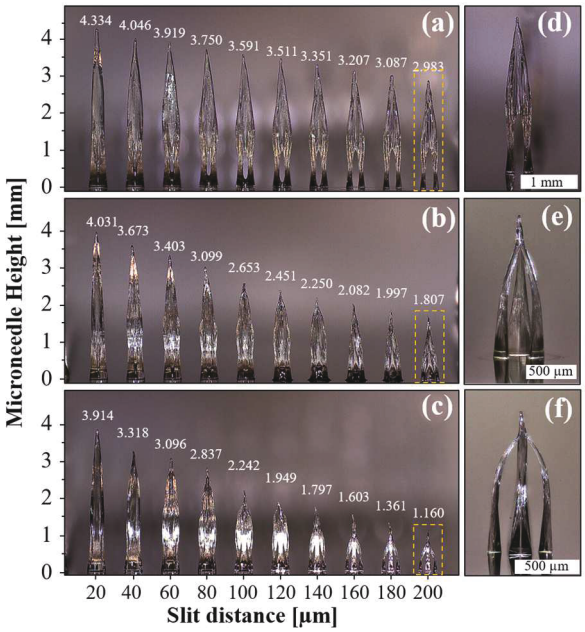

Fig. 4. Characterization result based on slit distance ranging from 20 to 200 µm. (a) Double-slit. (b) Triple-slit. (c) Quadruple-slit. Zoomed-in view of (d) Double-leg, (e) Triple-leg, and (f) Quadruple-leg microneedle.

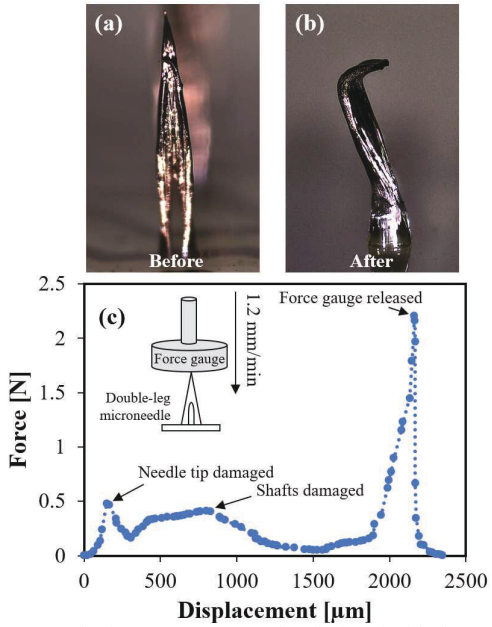

Fig. 5. Force displacement test result of the double-leg supported microneedle. (a) The shape of the double-leg supported microneedle, (b) the damaged tip after the force-displacement test, (c) the force-displacement behavior of the double-leg supported microneedle.

triple-, and quadruple-slit micro-patterns were patterned onto three different photomasks using a projection lithography system (SF-100 XPRESS, Scotech Co., Ltd.). The diameter of the micro-patterns was fixed at 500 µm while the slit distance was varied from 20 to 200 µm for all photomasks. A biocompatible liquid resin (Surgical guide resin, Formlabs Inc.) was chosen to fabricate the microneedle. A broadband UV mercury lamp was used as the light source (Model 30 UV light source, OAI Inc.), the intensity was set at 40 mW/cm^2 and 60 seconds of exposure time. Fig. 4 shows the characterization results of the multi-leg microneedle based on the described setup. Fig. 4(a) to (c) shows the characterization results of multi-leg microneedles focusing on the effect of slit distance. In brief, closer slit distances resulted in taller microneedles, albeit at the expense of leg separation. Based on the results, microneedles with a slit distance greater than 160 µm separated legs clearly while remaining intact. Fig. 4(d) to (f) shows the zoomed-in view of the microneedles with a constant slit distance of 200 µm but increasing number of slits. Given the same slit distance, micro-patterns with a greater number of slits form shorter microneedles in exchange for more supporting legs and sharper tip.

The double-leg supported microneedle with a height of 3 mm was characterized by the force-displacement equipment (FC200, Torbal Inc.) as shown in Fig. 5. The fabricated microneedle as shown in Fig. 5(a) was placed directly under the force gauge and the force gauge was moved down at a speed of 1.2 mm/min. The microneedle was compressed and damaged as shown in Fig. 5(b). During this test, the measured force was recorded every 1 millisecond. The total test time was converted into displacement in micrometer and plotted in Fig. 5(c). Three abrupt force reductions were observed during compression, which indicates the damage of the needle tip, supporting leg, and the release of the force gauge. The needle tip began to deform at 0.5 N without any mechanical failures, which has greatly exceeded the recommended minimum skin insertion force of 0.07 N for aged skin and 0.0278 N for young skin in the absence of an applicator [18]. The shaft of the microneedle started to be deformed after the tip damage. The compression force was linearly increasing at the double-leg position, indicating that the microneedle bodies still remained attached to the substrate. This characteristic result shows great potential for the use of the introduced microneedles as sensors and stimulating microdevices as well as the drug transportation method when the drug was coated into the microneedle.

The multi-leg microneedle was further developed as a local resistive micro-heater for potential thermal treatment use. Nine electrodes with a linewidth of 200 µm and prober pad size of 0.5×2 mm^2 were metal-patterned over a 3×3, 3-mm tall double-leg microneedle array using a shadow mask, DC sputtering, and electroplating process as shown in Fig. 6(a). Here, copper was used as the conductive material of the electrode, but it can be replaced with gold or platinum if biocompatibility is required for consideration. In this heat stimulating microneedle device, the copper thickness of the electrodes including the microneedle supporting legs was 5 µm thick while the copper thickness of the microneedle tip remained at 500 nm to create a resistance bump at the needle tip. This variation of copper thickness was achieved by selectively insulating the needle tip with a photoresist (NR26-25000P, Futurrex Inc.) during the electroplating process. Electrical current was applied to the prober pads of the microneedle device in the range of 0 to 1.2 A with a step size of 50 mA, and the thermal behavior was observed using a thermal camera (FLIR ETS320, Teledyne FLIR LLC) as shown in Fig. 6(b). In the thermal image, the microneedle showed the temperature of 60 °C where this temperature is often required in tissue engineering, while the electrodes and the prober pads showed slightly above the room temperatures. The thermal test

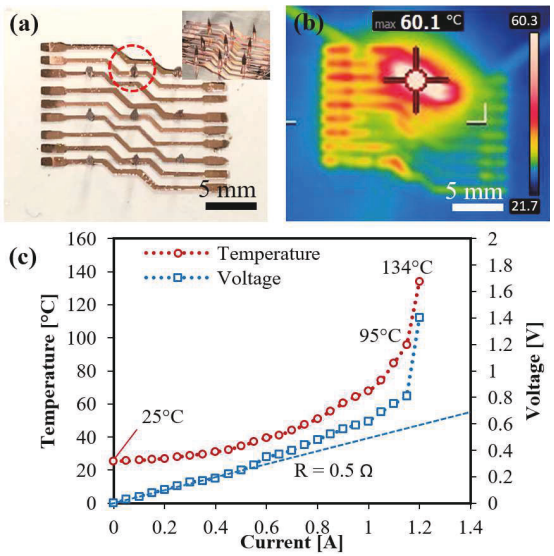

Fig. 6. Thermal performance of the micro-heater from 0 to 1.2 A. (a) 3 by 3 double-leg microneedle array, (b) thermal image of the microneedle, and (c) the temperature and voltage change in control of the current.

was further conducted by increasing the applied current and measured the corresponding temperature as well as the voltage. The highest useable temperature was observed at around 95 °C at the 0.8 V and 1.15 A. The nanometer thin copper at the needle tip completely burnt out at 1.2 A, showing a peak temperature of 134 °C.

IV. Conclusions

A multi-slit diffraction lithography has been introduced for the fabrication of leg-supported microneedles. A multi-slit diffraction created a shadow region between the two microslits that fabricated the two or more supporting legs of the microneedle. The diffracted lights from the multi slits above the shadow region were merged and formed the cone shape that was served as microneedle. In the paper, the distance between the slits and the slit numbers were investigated. The more slits and the longer distance created the shorter heights of the microneedle in general. The tallest microneedle was reported as 4.3 mm height with the double-leg supporting type, while the maximum four-leg supporting needles were successfully fabricated. The force-displacement test was conducted on the double-leg supporting microneedle and showed 0.5N as an initial insertion that exceeded the minimum recommended force of 0.07N as a microneedle. The double leg-supporting microneedle was also tested as a local heat stimulation device after selectively metalized. As the temperature of the 60 °C was typically required in the tissue related biomedical applications, the fabricated microneedle demonstrated the highest applicable temperature of 95 °C at approximately 1.15 A with 0.8 V operation parameters. The demonstrated multi-slit diffraction lithography can introduce various unique shapes of multi-leg supported microneedles and have a great potential to use in biomedical sensors and stimulation fields.

References

[1] R. S. J. Ingrole, E. Azizoglu, M. Dul, J. C. Birchall, H. S. Gill, and M. R. Prausnitz, "Trends of microneedle technology in the scientific literature, patents, clinical trials and internet activity," *Biomaterials*, vol. 267, p. 120491, Jan. 2021, doi: 10.1016/j.biomaterials.2020.120491.

[2] L. Zhao, Z. Wen, F. Jiang, Z. Zheng, and S. Lu, "Silk/polyols/GOD microneedle based electrochemical biosensor for continuous glucose monitoring," *RSC Adv.*, vol. 10, no. 11, pp. 6163–6171, Feb. 2020, doi: 10.1039/C9RA10374K.

[3] L. Rivas *et al.*, "Micro-needle implantable electrochemical oxygen sensor: ex-vivo and in-vivo studies," *Biosensors and Bioelectronics*, vol. 153, p. 112028, Apr. 2020, doi: 10.1016/j.bios.2020.112028.

[4] H. Park, W. Park, and C. H. Lee, "Electrochemically active materials and wearable biosensors for the in situ analysis of body fluids for human healthcare," *NPG Asia Mater*, vol. 13, no. 1, Art. no. 1, Mar. 2021, doi: 10.1038/s41427-020-00280-x.

[5] B. L. Zhang, X. P. Zhang, B. Z. Chen, W. M. Fei, Y. Cui, and X. D. Guo, "Microneedle-assisted technology for minimally invasive medical sensing," *Microchemical Journal*, vol. 162, p. 105830, Mar. 2021, doi: 10.1016/j.microc.2020.105830.

[6] L. Ren *et al.*, "Flexible microneedle array electrode using magnetorheological drawing lithography for bio-signal monitoring," *Sensors and Actuators A: Physical*, vol. 268, pp. 38–45, Dec. 2017, doi: 10.1016/j.sna.2017.10.042.

[7] Y. Liu, Q. Yu, X. Luo, L. Yang, and Y. Cui, "Continuous monitoring of diabetes with an integrated microneedle biosensing device through 3D printing," *Microsyst Nanoeng*, vol. 7, no. 1, Art. no. 1, Sep. 2021, doi: 10.1038/s41378-021-00302-w.

[8] Z. Faraji Rad, P. D. Prewett, and G. J. Davies, "High-resolution two-photon polymerization: the most versatile technique for the fabrication of microneedle arrays," *Microsyst Nanoeng*, vol. 7, no. 1, Art. no. 1, Sep. 2021, doi: 10.1038/s41378-021-00298-3.

[9] Z. Chen *et al.*, "Rapidly Fabricated Microneedle Arrays Using Magnetorheological Drawing Lithography for Transdermal Drug Delivery," *ACS Biomater. Sci. Eng.*, vol. 5, no. 10, pp. 5506–5513, Oct. 2019, doi: 10.1021/acsbiomaterials.9b00919.

[10] Y. Bozkurt and E. Karayel, "3D printing technology; methods, biomedical applications, future opportunities and trends," *Journal of Materials Research and Technology*, vol. 14, pp. 1430–1450, Sep. 2021, doi: 10.1016/j.jmrt.2021.07.050.

[11] S. F. Shiba, H. Jeon, J.-S. Kim, J.-E. Kim, and J. Kim, "3D Microlithography Using an Integrated System of 5-mm UV-LEDs with a Tilt-Rotational Sample Holder," *Micromachines*, vol. 11, no. 2, Art. no. 2, Feb. 2020, doi: 10.3390/mi11020157.

[12] J. Kim, Y.-K. Yoon, and M. G. Allen, "Computer numerical control (CNC) lithography: light-motion synchronized UV-LED lithography for 3D microfabrication," *J. Micromech. Microeng.*, vol. 26, no. 3, p. 035003, Jan. 2016, doi: 10.1088/0960-1317/26/3/035003.

[13] J. Kim, "Fabrication of SU-8 Microtowers for a 100-Turn Toroid Inductor," in *2018 IEEE 13th Annual International Conference on Nano/Micro Engineered and Molecular Systems (NEMS)*, Apr. 2018, pp. 389–392. doi: 10.1109/NEMS.2018.8556894.

[14] J. Kim, X. Cheng, H. Ahn, D. S. Elles, and Y.-K. Yoon, "Lithographically defined integrable air-lifted bow-tie antennas," in *2010 IEEE 23rd International Conference on Micro Electro Mechanical Systems (MEMS)*, Jan. 2010, pp. 791–794. doi: 10.1109/MEMSYS.2010.5442287.

[15] J. Y. Tan, A. Kim, and J. 'JK' Kim, "Modeling, characterization, and fabrication of bell-tip microneedle array by diffraction and self-aligned lens effects," *Appl. Phys. Lett.*, vol. 119, no. 2, p. 023501, Jul. 2021, doi: 10.1063/5.0055073.

[16] J. Y. Tan, A. Kim, and J. Kim, "Fabrication and Characterization of Hollow Microneedle Array using Diffraction UV Lithography," presented at the 2021 Transducers - 2021 21st International Conference on Solid-State Sensors, Actuators and Microsystems (TRANSDUCERS), Jun. 2021.

[17] J. Y. Tan, M. Ahn, H. Al-Thuwaini, S. Choi, and J. J. K. Kim, "Diffraction Lithography for 3-D Microneedle Fabrication," in *2020 IEEE 33rd International Conference on Micro Electro Mechanical Systems (MEMS)*, Jan. 2020, pp. 921–924. doi: 10.1109/MEMS46641.2020.9056456.

[18] O. Olatunji, D. B. Das, M. J. Garland, L. Belaid, and R. F. Donnelly, "Influence of Array Interspacing on the Force Required for Successful Microneedle Skin Penetration: Theoretical and Practical Approaches," *Journal of Pharmaceutical Sciences*, vol. 102, no. 4, pp. 1209–1221, Apr. 2013, doi: 10.1002/jps.23439.